

Role of microstructure on contact damage and strength degradation of micaceous glass-ceramics

Irene M. Peterson¹, Sataporn Wuttiphon¹, Brian R. Lawn¹, Kenneth Chyung²

¹Materials Science and Engineering Laboratory, National Institute of Standards and Technology, Gaithersburg, Maryland, USA

²Corning Incorporated, Glass and Glass-Ceramic Research, Corning, NY 14831, USA

ABSTRACT

Objectives. This study examines the hypothesis that microstructure plays a critical role in the accumulation of strength-degrading damage in dental ceramics. A series of micaceous glass-ceramics crystallized from a common glass composition, using heat treatments to increase the diameter and aspect ratio of mica platelets, is used as a model ceramic system.

Methods. Damage modes are investigated by Hertzian contact testing. Four-point bend tests on indented specimens quantify the influence of single-cycle and multi-cycle damage on strength.

Results. Two competing damage modes are observed: fracture, by tensile-induced cone cracking at the macroscopic level; and quasi-plastic deformation, by shear-induced yield at the microscopic level. The quasi-plastic mode becomes more dominant as the microstructures become coarser and more elongate. Bend tests show severe strength losses in the finer grain structures where cone cracking dominates, but relatively small losses in the coarser grain structures where quasi-plasticity dominates. Whereas natural strengths decline with increasing crystallization temperature, the strengths after indentation damage attain a maximum at intermediate crystallization temperatures. Multiple-cycle contact loading reduces strengths even further, and at relatively low indentation loads, indicating susceptibility to fatigue. Finite element modelling is carried out to evaluate the stress components that drive the damage modes.

Significance. Microstructure is confirmed to be a controlling factor in determining the nature and degree of strength-impairing damage accumulation in dental ceramics. The Hertzian test provides a means of characterizing such damage in the context of clinical function.

© 1998 Academy of Dental Materials. Published by Elsevier Science Ltd

INTRODUCTION

All-ceramic dental restorations are attractive for their aesthetic appeal. One group of dental ceramics that has high aesthetics and has been used in crowns, inlays and onlays is the micaceous glass-ceramics (Chyung *et al.*, 1972, 1974; Grossman, 1991). These ceramics were originally designed for easy machinability, by incorpor-

ating weak interfaces between mica platelets and glass matrix (Chyung *et al.*, 1972, 1974). It is well documented that the size and shape of the mica platelets determine other clinically relevant mechanical properties, such as strength, wear and fatigue resistance (Chyung *et al.*, 1972, 1974; Grossman, 1991; Cai *et al.*, 1994b; Nagarajan and Jahanmir, 1996; Xu *et al.*, 1996). However, systematic studies of the role of glass-ceramic microstructure on damage accumulation under contact conditions that simulate oral function are only recently beginning to appear in the literature (Denry and Rosenstiel, 1995; Denry *et al.*, 1996; Fischer-Cripps and Lawn, 1996b; Peterson *et al.*, 1998).

In oral environments, dental restorations may be subjected to masticatory forces of more than 200 N over a lifetime of more than 10^7 cycles (DeLong and Douglas, 1983; Anusavice, 1989; Phillips, 1991; Craig, 1997), at contacts between opposing cusps of characteristic radii of 2–4 mm (Wheeler, 1958). The contact damage produced under such conditions is most closely simulated by indentation with a hard sphere, the so-called Hertzian test (Hertz, 1896). As recently demonstrated (Peterson *et al.*, 1998), this test can reveal essential information on damage modes under clinically relevant conditions. In ideally brittle materials the damage consists of a macroscopic cone crack, which initiates from an embryonic surface ring crack *outside* the indentation site (Roesler, 1956; Frank and Lawn, 1967; Langitan and Lawn, 1969; Mikosza and Lawn, 1971; Wilshaw, 1971; Lawn and Wilshaw, 1975). In tougher ceramics the damage consists of a “quasi-plastic” zone containing microscopic shear faults and microcracks *beneath* the indentation site (Guiberteau *et al.*, 1993; Cai *et al.*, 1994b; Guiberteau *et al.*, 1994; Lawn *et al.*, 1994; Pature and Lawn, 1994). Microstructure is the key factor governing the balance between these two competing modes.

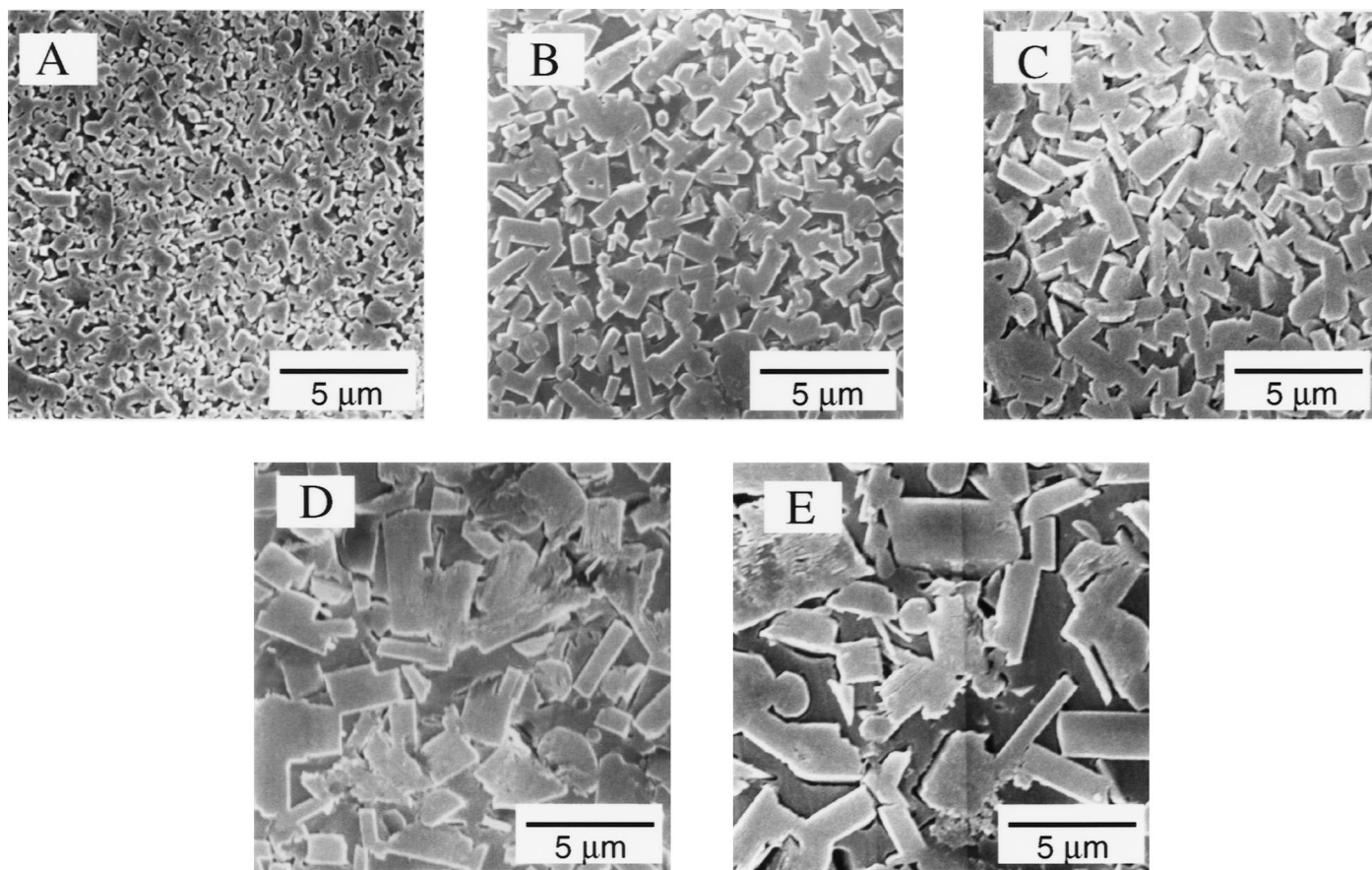


Fig. 1. Scanning electron micrographs showing microstructures of micaceous glass-ceramic (MGC) materials: A. F ("fine"), B. FM ("fine-medium"), C. M ("medium"), D. MC ("medium-coarse"), E. C ("coarse"). Surfaces etched with 10 wt% ammonium bifluoride in water for 20 s to reveal mica platelets in glass matrix, and gold coated. Secondary electron images. Micrographs A, C and E from Peterson *et al.* (1998).

In this paper we investigate the role of microstructure on contact damage and attendant strength degradation in micaceous glass-ceramics, in the context of oral function. We conduct an experimental and computational analysis of the damage modes in a series of controlled microstructures in which simple heat treatments are used to change the size and shape of the mica platelets within the glass matrix. Single-cycle contact tests are conducted to examine the transitions from cracking to quasi-plasticity that attend microstructural coarsening, and to measure critical loads for initiation of both of these damage modes. Multi-cycle contact tests are used to observe how the damage accumulates in the different microstructures under fatigue conditions. A feature of the study is the use of strength tests to quantify the material degradation associated with both single-cycle and multi-cycle contact damage. Implications of the results concerning clinical relevance are discussed.

MATERIALS AND METHODS

Materials preparation and characterization. A series of micaceous glass-ceramic (MGC) blocks, based on a K_2O - MgF_2 - MgO - SiO_2 composition (Chyung *et al.*, 1972, 1974; Grossman, 1991), was prepared. These blocks were crystallized from the base glass by

controlled heat treatments at 1000, 1040, 1060, 1080 and 1120°C for 4 h (Grossman, 1991; Fischer-Cripps and Lawn, 1996a). The composition used here (Grossman, 1991) is the same as that used to make commercial Dicor (Dentsply/Caulk, Milford, DE) for inlays, onlays and crowns, although in Dicor coloring agents are added. After firing, the blocks were machined into 3 mm × 4 mm × 50 mm bars for testing.

Microstructures of these MGC materials have been described in earlier studies (Fischer-Cripps and Lawn, 1996a; Peterson *et al.*, 1998). In those studies, specimens were surface polished with diamond paste to a 0.5 μm finish and acid etched. SEM micrographs of the microstructures are shown in Fig. 1. For convenience, we designate the microstructures in Fig. 1 as F, FM, M, MC and C (F—fine, M—medium, and C—coarse). Observe the nearly contiguous network of hexagonal blocky mica platelets within the glass matrix. Sizes, shapes and volume fractions of mica platelets have been measured in a previous study using linear intercept analyses (Fischer-Cripps and Lawn, 1996a): the diameter of the platelets increases monotonically from 1.0 to 10 μm over the temperature range, and the aspect ratio (diameter/thickness) from 3 to 9; the volume fraction of platelets is relatively invariant at 0.60–0.70 over this same temperature range.

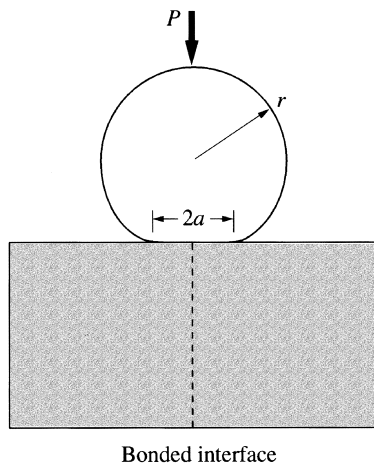


Fig. 2. Schematic of Hertzian contact test. Hard sphere, radius r , loaded with force P onto specimen surface, producing contact radius a . Specimen may be pre-sectioned in bonded-interface configuration (dashed line) to reveal subsurface damage.

The presence of quasi-plasticity in the contact response of such microstructures is most graphically demonstrated on indentation stress–strain plots using the Hertzian test (Fig. 2) (Cai *et al.*, 1994b). Such plots are constructed by measuring the contact radius a as a function of load P for each given sphere radius r , and plotting indentation stress, $p_0 = P/\pi a^2$, against indentation strain, a/r . Plots for our MGC materials are shown in Fig. 3, from an earlier study (Fischer-Cripps and Lawn, 1996a)—data for the brittle base glass from which the MGC materials are crystallized are included as a baseline linear response. These plots provide us with a basis for later stress analysis of damage patterns.

Hertzian contact damage. A systematic study of the damage modes in each of the MGC microstructures was made using the Hertzian test in Fig. 2. A hard tungsten carbide (WC) sphere of radius r was mounted on the underside of the crosshead of a loading machine. The crosshead was lowered until the sphere contacted the specimen, and the load increased monotonically to a peak value P . Two types of loading condition were used: single-cycle loading at a fixed load–unload crosshead speed of 0.2 mm min^{-1} (Instron 1122, Canton, MA); and multi-cycle loading at a frequency of 10 Hz (Instron 8502, Canton, MA). All contact tests were done in air.

Fracture and quasi-plasticity subsurface contact damage patterns were examined by optical microscopy using a “bonded interface” configuration (Fig. 2), based on a modification of a procedure originally devised for metals (Mulhearn, 1959). This procedure has been outlined elsewhere for ceramics (Cai *et al.*, 1994b; Guiberteau *et al.*, 1994; Peterson *et al.*, 1998). The bonded-interface specimen is produced by first polishing two half-bars with diamond paste to a $0.5 \mu\text{m}$ finish. The two polished surfaces are bonded together using a thin layer ($<5 \mu\text{m}$) of a cyanoacrylate-based adhesive (Loctite, Newington, CT). The top and bottom surfaces of the adhered half-bars are ground flat, and the top surface polished with diamond paste to a $0.5 \mu\text{m}$ finish.

Indentations are made on the top surfaces of the specimens in a row along the carefully aligned interface (Peterson *et al.*, 1998), using a WC sphere of radius $r = 3.18 \text{ mm}$. After indentation testing, the adhesive is dissolved in acetone. The separated surfaces are coated with gold and viewed in the optical microscope using Nomarski interference contrast.

Critical indentation loads for the onset of cone cracking, P_C , and yield, P_Y , were measured in single-cycle loading for all five MGC materials, again using WC spheres of radius $r = 3.18 \text{ mm}$. P_C was measured by viewing the indented surfaces with Nomarski interference contrast in an optical microscope. An acoustic sensor attached to the surface of the specimen during indentation was used to detect signals associated with any unstable formation of full cone cracks from embryonic surface ring cracks (Mikosza and Lawn, 1971). P_Y was measured by similarly viewing the indented surfaces, as the lowest load that causes a detectable surface impression (Davies, 1949). Application of a gold coating to the indented surfaces improved the visibility of the cracks and quasi-plastic impressions. Means and standard deviations of the critical loads were calculated from a minimum of five indentations per load per specimen.

Finite element modelling. A finite element model (FEM), using a commercial package (Strand, G&D Computing, Sydney, Australia), was used to simulate the contact in Fig. 2, at a fixed sphere radius $r = 3.18 \text{ mm}$. Details of the FEM algorithm used are described elsewhere (Fischer-Cripps and Lawn, 1996b). In the calculation, loading proceeds from initial contact in a stepwise manner, enabling determination of contact radius a at each load increment P , and allowing in turn for computation of indentation stresses ($p_0 = P/\pi a^2$) and strains (a/r). Plastic deformation in the test material is governed by a critical shear stress criterion. All grid volume elements are allowed to deform in accordance with a generic bilinear elastic–plastic constitutive stress–strain relation $\sigma(\epsilon)$ in uniaxial compression (Fischer-Cripps and Lawn, 1996b; Lawn and Marshall, 1998):

$$\sigma = E\epsilon \quad (\sigma < Y) \quad (1a)$$

$$\sigma = Y + \alpha(\epsilon E - Y) \quad (\sigma > Y) \quad (1b)$$

where E is Young’s modulus, Y the uniaxial stress for the onset of yield, and α a dimensionless strain-hardening coefficient in the range $0 \leq \alpha \leq 1$ ($\alpha = 0$, fully plastic; $\alpha = 1$, fully elastic). The material parameters in Eqs (1a) and (1b) are composite values for the two-phase microstructures, appropriate to continuum calculations of macroscopic yield properties of interest here.

Values for the parameters in Eqs (1a) and (1b) were obtained for our MGC materials as follows: E , using sonic velocity measurements (Fischer-Cripps and Lawn, 1996a); Y , from the relation $P_Y \approx 1.1\pi a^2 Y$, derived from the condition that the maximum shear stress in the contact field exceeds $Y/2$ (Tabor, 1951; Lee *et al.*, 1997), with a measured directly at $P = P_Y$ (previous subsection); and α , from best fits of Eqs (1a)

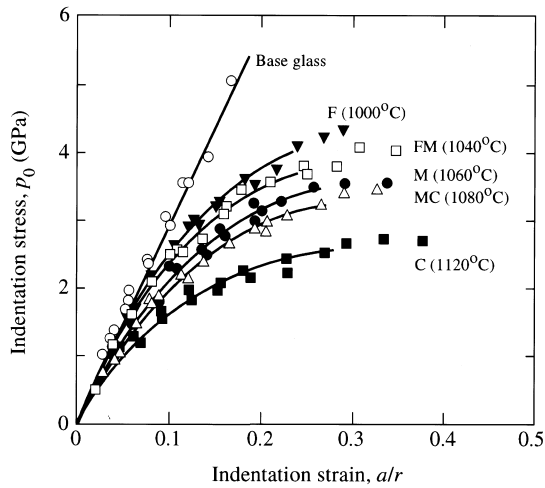


Fig. 3. Indentation stress-strain curves for MGC materials, including base glass, using WC spheres. Data from Fischer-Cripps and Lawn, 1996a. Solid curves from FEM analysis.

and (1b) to the actual indentation stress-strain data in Fig. 3, determined to an accuracy of ± 0.05 (Fischer-Cripps and Lawn, 1996b). Note that the abrupt discontinuity in slope at the yield point in Eqs (1a) and (1b) is smoothed out at the corresponding yield point in the indentation stress-strain curves of Fig. 3, owing to strong elastic confinement of the incipient quasi-plastic zone in the initial stage of development beneath the contact (Tabor, 1951; Fischer-Cripps and Lawn, 1996a; Fischer-Cripps and Lawn, 1996b).

With these parameters calibrated, the FEM algorithm was used to evaluate principal shear and tensile stresses and strains within the contact field.

Strength testing. The effect of single-cycle contact damage on strength was measured for all five MGC materials by breaking bar specimens in four-point bending. Prior to indentation, the bars were surface polished and chamfered to remove edge flaws. Indentations were made with a WC sphere of $r = 3.18$ mm, at peak loads up to $P = 2500$ N. The bars were placed in the four-point bend fixture (inner span 10 mm, outer span 20 mm) with the indentation

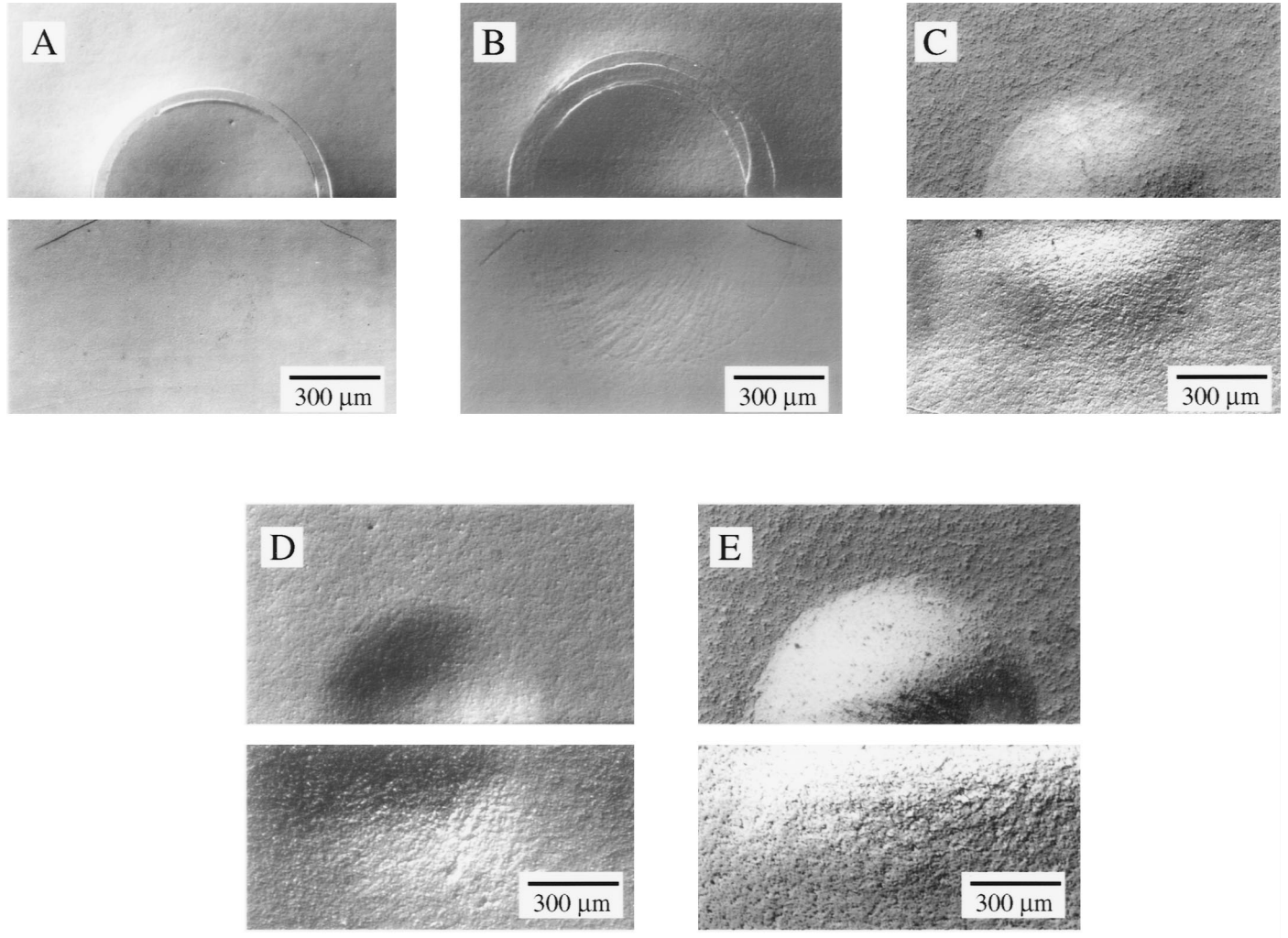


Fig. 4. Optical micrographs (Nomarski illumination) of damage in bonded-interface specimens of MGC: A, F, B, FM, C, M, D, MC, E. C. Showing half-surface (upper) and section (lower) views, single-cycle indentations with WC sphere, $r = 3.18$ mm and $P = 1000$ N. Cone cracking and quasi-plasticity damage are evident. Micrographs A, C and E from Peterson *et al.* (1998).

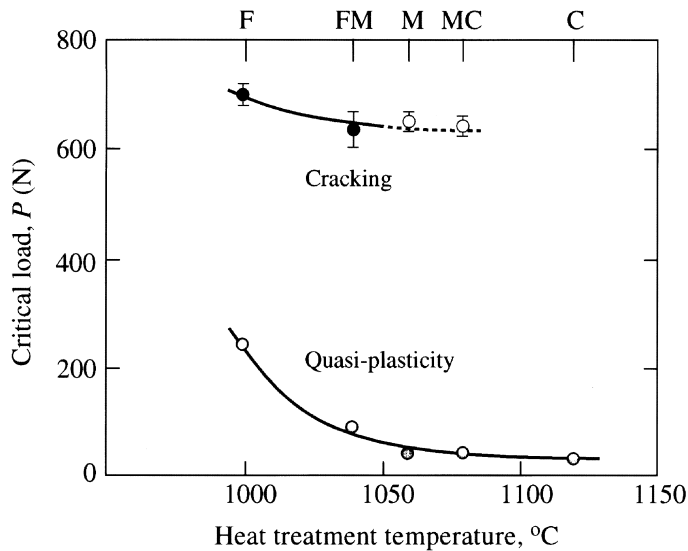


Fig. 5. Critical loads for onset of surface cone cracking (P_C) and subsurface yield (P_Y) for MGC materials. Data plotted as function of crystallization temperature, at fixed WC sphere radius $r = 3.18$ mm. Open symbols for $P_C(r)$ data indicate surface ring cracks only.

centered on the tensile side. After placing a drop of silicone oil onto the indentation site, the bars were broken in fast fracture (fracture time < 40 ms), to minimize the effects of moisture on the strength (Marshall and Lawn, 1980). Strengths were calculated from the breaking loads using beam theory. Three to five specimens were broken at each load, and means and standard deviations calculated.

The effect of multi-cycle indentation on strength degradation (“contact fatigue”) was evaluated for F-MGC, M-MGC and C-MGC materials, at a sphere radius $r = 3.18$ mm, up to $n = 10^6$ cycles (Guiberteau *et al.*, 1993; Cai *et al.*, 1994a). A load $P = 500$ N below the threshold for cone crack initiation in single-cycle loading was chosen for this series of tests.

Comparative strength tests were run on specimens after sandblasting with $50 \mu\text{m}$ silica particles, under a gas pressure of 0.5 MPa at a nozzle-specimen distance of 10 mm, to simulate clinical dental preparation protocols.

RESULTS

Experimental results. Views of surface and subsurface damage from bonded-interface patterns for each MGC material are shown in Fig. 4, from indentations at $P = 1000$ N with a sphere radius $r = 3.18$ mm. The sequence shows an evolution in the competition between cracking and deformation, as follows: A. F-MGC—the response is predominantly brittle, with a well-developed cone crack. However, there is also a slight depression within the crack periphery, indicating some quasi-plastic yielding. B. FM-MGC—the cone crack is less well developed, and the quasi-plastic zone is more apparent. C. M-MGC—the cone crack is suppressed—only a surface ring crack remains (note the absence of any downward extension in the section view). The surface impression is deeper, and the subsurface

TABLE 1: YIELD PARAMETERS FOR MATERIALS USED IN FINITE ELEMENT MODELLING, γ FROM CRITICAL CONTACT PRESSURE AT FIRST YIELD AND α FROM FEM BEST FIT TO INDENTATION STRESS-STRAIN DATA

Material	Yield stress γ (GPa)	Strain-hardening coefficient α
F-MGC	1.63	0.80
FM-MGC	1.19	0.60
M-MGC	0.91	0.50
MC-MGC	0.91	0.40
C-MGC	0.83	0.20

quasi-plastic zone is now well developed. D. MC-MGC—the ring cracks are now vestigial, and the surface impression and subsurface quasi-plastic zone are further developed. E. C-MGC—any vestigial ring cracks are now almost invisible. The quasi-plastic zone is totally dominant, reminiscent of hardness impressions in metals.

Critical loads for the onset of cracking and yield damage in each of the MGC materials are plotted in Fig. 5 as a function of crystallization temperature. Observe that $P_C \gg P_Y$ over the entire temperature range, confirming that quasi-plasticity is readily produced in all microstructures. With the P_C data, the solid symbols for F-MGC and FM-MGC indicate generation of full cone cracks, the open symbols for M-MGC and MC-MGC indicate surface ring cracks only (no point is included for the essentially plastic C-MGC). The insensitivity of P_C to heat-treatment temperature is of less consequence than the reduction in crack severity. With the P_Y data, the yield stress initially diminishes quickly through F to M, and then saturates through M to C at a relatively low value as the quasi-plastic mode becomes dominant.

Analysis of contact fields. An FEM analysis of the contact fields was carried out using the following parameters: for the MGC, common Young’s modulus $E = 70$ GPa and $\nu = 0.26$ (Fischer-Cripps and Lawn, 1996b) along with measured yield stresses Y and best-fit values α (Table 1); for the WC indenter, $E = 614$ GPa, $\nu = 0.22$, $Y = 6.0$ GPa and $\alpha = 0.10$ (Fischer-Cripps and Lawn, 1996b). The FEM-regenerated stress-strain functions are included as the solid curves in Fig. 3. The trend to more pronounced nonlinearity (increasing α) with increasing microstructural coarsening correlates with the intensity of quasi-plastic deformation observed in the micrographs in Fig. 4.

Given the calibrated parameters in Table 1, the FEM algorithm can be used to evaluate the contact fields. Accordingly, Fig. 6 maps out principal shear components, for $P = 1000$ N, i.e. corresponding to conditions in Fig. 4. Fig. 6 plots shear strain contours,

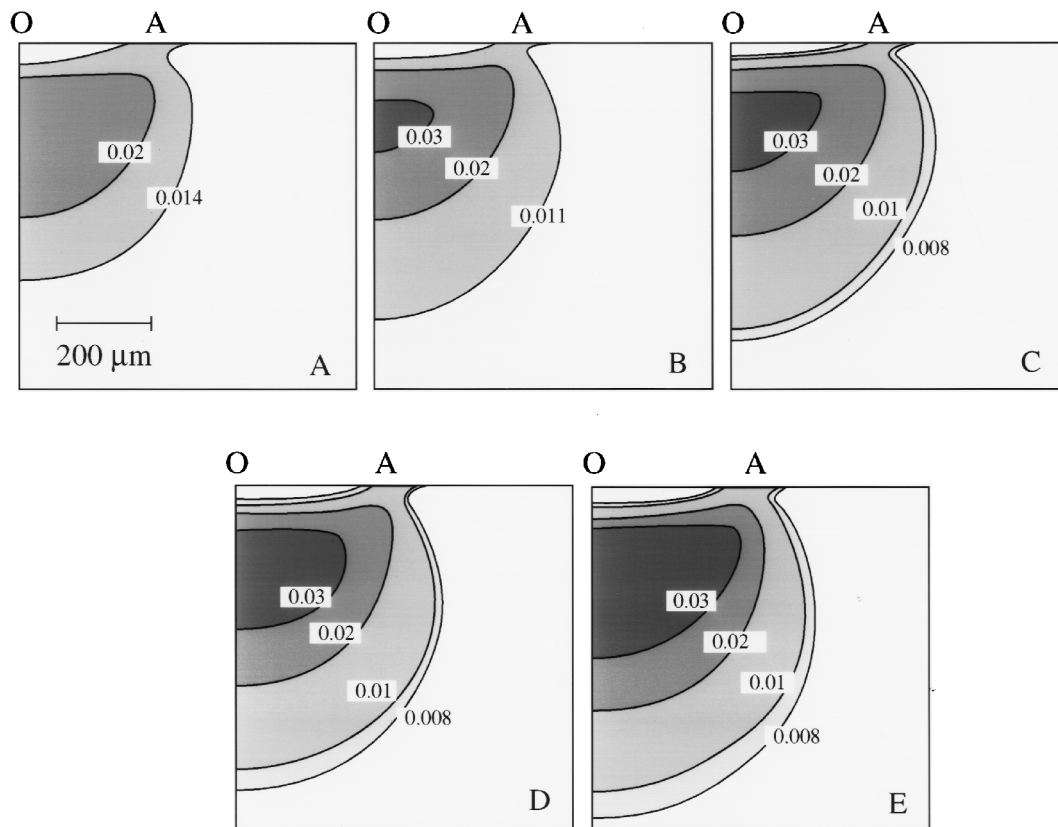


Fig. 6. FEM-generated maximum shear strain contours within yield zone boundaries (shaded), for indentation of MGC materials with WC sphere, radius $r = 3.18$ mm, load $P = 750$ N: A. F, B. FM, C. M, D. MC, E. C. Contact radius OA. Compare quasi-plastic zones in micrographs in Fig. 4.

where the shaded areas indicate the regions within which yield occurs and the degree of shading indicates levels of strain. In this instance, contours of *strain* rather than *stress* are plotted to afford a direct correlation with the observed damage intensity in the micrographs (bearing in mind that the Nomarski contrast used in Fig. 4 is *displacement-sensitive*) (Lee *et al.*, 1997). The geometries and intensities of the predicted damage zones in Fig. 6 reproduce the main features of the experimental observations in Fig. 4, confirming quasi-plasticity as a shear-driven process. Note in particular how the strain contours become progressively more intense through the sequence F–FM–M–MC–C.

The FEM calculations enable parallel evaluations of the tensile stress fields. At the same load $P = 1000$ N as used in Fig. 6, the maximum tensile stress in the top surfaces varies over only a small range (1.0–1.1 GPa) with changing microstructure. This result is consistent with the insensitivity of P_C data to crystallization temperature in Fig. 5.

Single-cycle damage. Strengths of MGC specimens subjected to single-cycle contacts are plotted in Fig. 7 as a function of contact load P . Included at right are optical micrographs of four-point bend failures from contact sites, at $P = 1500$ N: in the F, FM and M materials the surface traces of the breaks lie outside the contact, and move progressively toward the surface ring, characteristic of failures from the bases

of ever-shallower cone cracks (Lawn *et al.*, 1984); in the MC material, breaks initiate sometimes from ring cracks (as in Fig. 7D), but more often from the quasi-plastic zones, indicating transitional behavior; in the C material the breaks pass closer to the center of the contact, intersecting the contact periphery almost orthogonally, consistent with subsurface failure initiation from within the quasi-plastic zone (Lawn *et al.*, 1998).

In the strength plots, closed symbols represent failures from cone or ring cracks, grey symbols from quasi-plasticity zones, open symbols from other origins. Boxes at the left axis represent strengths of unindented, polished specimens. Vertical dashed lines indicate critical loads, P_C , for cracking (where applicable) and P_Y for yield. Solid curves are empirical data fits. The F, FM and M materials exhibit typical brittle responses: no perceptible degradation at $P < P_C$, indicating failures from natural flaws; abrupt dropoff at $P = P_C$, highlighting the effectiveness of cone cracking as a source of strength degradation; and continued falloff at $P > P_C$, but at a relatively slow rate, as the cone cracks are driven deeper with ever-increasing load. Observe that the incidence of accompanying plasticity at $P > P_Y$ ($< P_C$) has no apparent effect on the strength in F and FM. The MC and C materials exhibit more quasi-plastic responses: no degradation at loads P up to and beyond P_Y ; gradual falloff at some load $P \gg P_Y$.

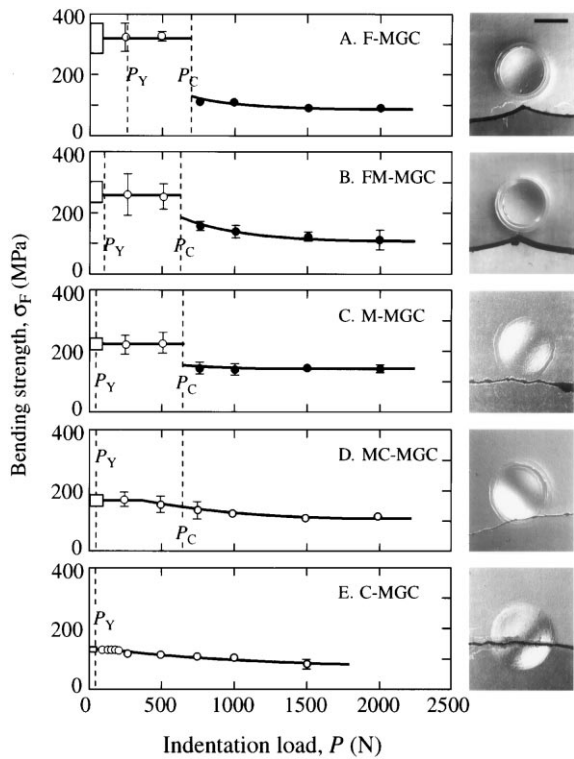


Fig. 7. Strengths of MGC specimens as function of contact load. Single-cycle indentations with WC sphere, $r = 3.18$ mm. Data points are means and standard deviations, 3–5 flexure specimens per point: closed symbols represent failures from cone cracks, grey symbols failures from quasi-plasticity zones, open symbols from other origins. Open boxes at left axis represent strengths of polished, unindented specimens. Vertical dashed lines indicate critical loads for cracking and yield. Solid curves are empirical fits to the data. Included at right are optical micrographs (Nomarski illumination) showing surface views of contact failure sites in MGC bend specimens (tension axis vertical), at $P = 1500$ N (marker in (A) is $500 \mu\text{m}$).

It is instructive to replot some of the data in Fig. 7 as a function of crystallization temperature, to highlight the role of microstructure on strength behavior. The plot in Fig. 8 compares strength data for specimens in the as-polished (unindented) state with data from specimens with single-cycle contact damage at load $P = 750$ N, along with some data from sandblast-damaged specimens. The pristine strengths decline monotonically with rising crystallization temperature, consistent with a scaling in flaw size associated with the weak mica–glass interfaces in the progressively coarsening microstructures (Fig. 1) (Lawn, 1993). The strengths of the indented specimens are degraded relative to the pristine strengths over the entire range of temperatures: most markedly at the lowest temperatures (F), moderately at the intervening temperatures (M), and barely at all at the highest temperatures (C). A distinctive feature of the strength data for the damaged specimens is a maximum somewhere between the FM and M materials. The considerable strength degradation in the finer F and FM materials is attributable to the presence of well-developed cone cracks. The strength losses are comparatively minor in the coarser MC and C materials, reflecting the greater damage tolerance associated with quasi-plastic contacts. In a clinical context, it is notable that the data from the sandblast

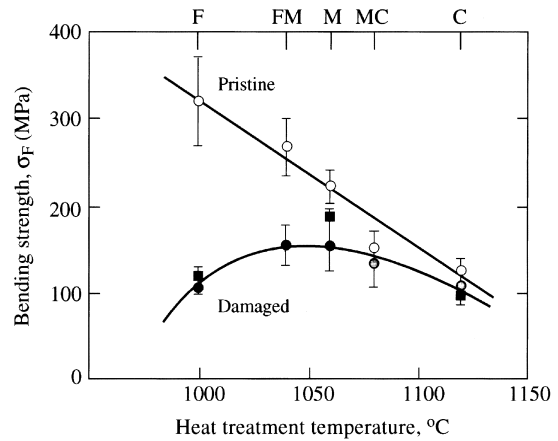


Fig. 8. Strength versus crystallization temperature for MGC materials. Data replotted from Fig. 7: strengths of pristine (as-polished, unindented) specimens, breaks from natural flaws (open circles); strengths of indented specimens, $r = 3.18$ mm at load $P = 750$ N, breaks from cracks (closed circles) and quasi-plastic damage zones (grey circles); strengths of sandblasted specimens (squares). Solid curves are empirical fits to the data.

treatment overlap the indentation data within the standard deviation scatter (Fig. 8), suggesting that the contact test is an appropriate indicator of the damage intensity incurred in common abrasive finishing procedures.

ANOVA on the data in Fig. 7 shows that the strength decrements at $P = 1500$ N relative to the intrinsic (as-polished) values are significant in all cases ($p < 0.05$). *Multi-cycle damage.* Fig. 9 shows optical micrographs of multi-cycle contact sites in F, M and C surfaces after $n = 10^6$ cycles at a load $P = 500$ N. Cycling dramatically increases the damage severity in all three materials, from initially shallow quasi-plastic indentations with no visible sign of cracking (not shown) to much deeper indentations with distinctive crack patterns and annular surface “fretting” (Johnson, 1985). The induced crack patterns differ in form, from well-developed cones in F to shallow surface rings in M and no significant ring cracks at all (but most severe annular fretting) in C. Incipient radial cracks (Lawn and Wilshaw, 1975) are observed at the edges of the surface damage patterns in F and C, but not in M.

Strengths of MGC specimens subjected to multi-cycle contacts are shown in Fig. 10 as a function of number of cycles n , at $P = 500$ N. Again, the F material shows a typical “brittle” response, with abrupt strength falloff at $n = 10^2$ – 10^3 . Fractographic examination of broken specimens confirmed the association of this falloff with the appearance of large cone cracks. The M material also shows a brittle response, but with markedly smaller falloff at $n = 1$ – 10 . This still abrupt but smaller falloff is consistent with the fractographic observations, which indicated failures from much shallower, barely visible ring cracks. The C material shows a “quasi-plastic” response, with an immediate but gradual fall off in strength after the first cycle. In this case fractography confirmed that the failures occur from quasi-plastic zones over the entire data range. The radial cracks observed in the F and C materials (Fig. 9)

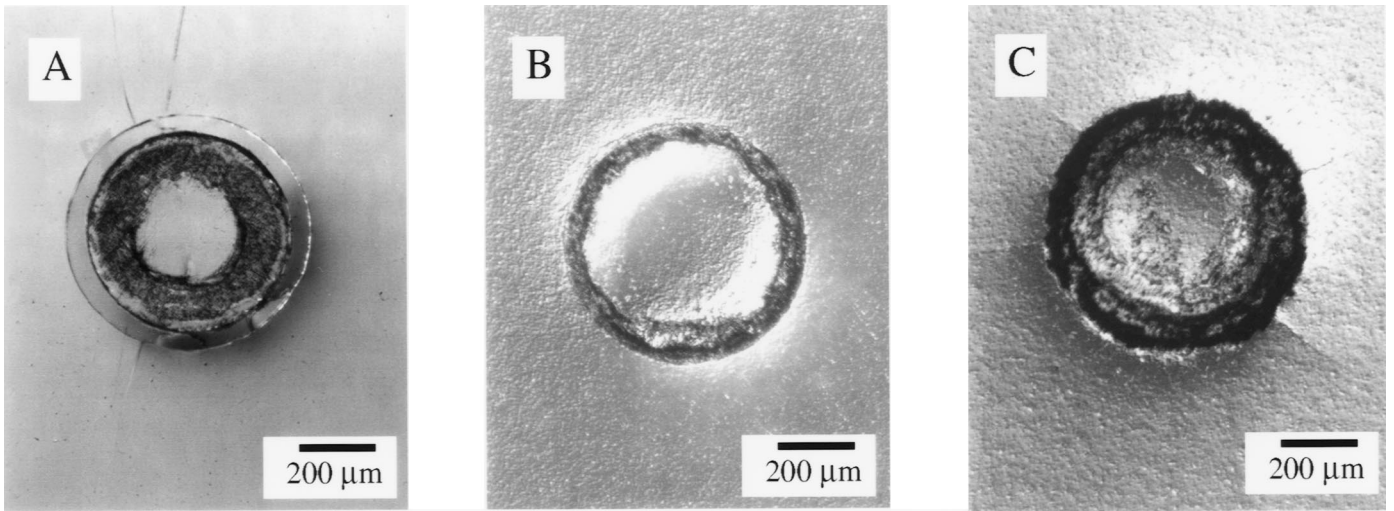


Fig. 9. Optical micrographs (Nomarski illumination) showing surface views of contact sites in MGC specimens: A. F, B. M, and C. C. Multi-cycle indentations, $n = 10^6$ cycles, with WC sphere $r = 3.18$ mm at load $P = 500$ N.

do not appear to be sufficiently developed to act as failure sites.

DISCUSSION

We have used the Hertzian contact test to identify damage modes in a micaceous glass-ceramic with microstructures controlled by crystallization heat treatments (Fig. 4). Two competing damage modes have been identified: brittle, by tensile-induced cone cracking; and quasi-plastic, by shear-induced yield. Cone cracking is more strongly developed in the finer grain structures (lower crystallization temperatures), and is virtually suppressed in the coarser grain structures (higher crystallization temperatures). This suppression has been attributed to two causes: relaxation of the subsurface tensile zones outside the contact from the quasi-plasticity (Fischer-Cripps and Lawn, 1996b); and enhanced deflection of surface ring cracks away from tensile stress trajectories (Lee *et al.*, 1997). Quasi-plasticity is more strongly developed in the coarser grain structures, but is present in all cases. These trends are consistent with reports of microstructurally-induced “brittle–ductile” transitions in other ceramic systems (Lawn *et al.*, 1994). Strength degradation of bar specimens with single-cycle contact damage is highly sensitive to damage mode—severe in the finest (F) materials with dominant cone cracks, slight in the coarsest (C) materials with dominant quasi-plasticity zones (Fig. 7). On the other hand, once damage is introduced, the degradation is relatively insensitive to the contact load—or even to the means by which the damage is introduced, e.g. by indentation or sandblasting (Fig. 8) or machining (Grossman, 1991). The strength degradation is further enhanced in specimens with multi-cycle contacts (Fig. 10). Intermediate (M) materials appear to be most tolerant to cyclic damage accumulation, with highest retained strengths, at least at the contact load (500 N) and radius (3.18 mm) studied.

FEM has been used to evaluate the contact stress states associated with the damage modes, using a

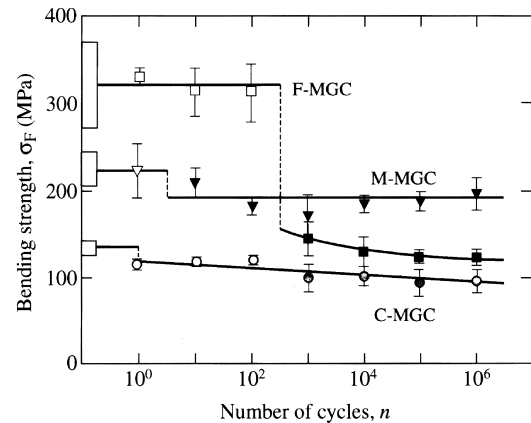


Fig. 10. Strengths of MGC specimens as function of number of contact cycles. Multi-cycle indentations with WC sphere, $r = 3.18$ mm, fixed contact load $P = 500$ N. Data points are means and standard deviations, 3–5 flexure specimens per point: closed symbols represent failures from cone cracks, grey symbols failures from quasi-plasticity zones, open symbols from other origins. Open boxes at left axis represent strengths of polished, unindented specimens. Solid curves are empirical fits to the data.

bilinear elastic–plastic constitutive law. Shear strain contours (Fig. 6) demonstrate the capacity of FEM to account for essential features of the macroscopic quasi-plastic zone geometry and damage intensity. Analytical fracture mechanics models (Lawn *et al.*, 1998) are currently being developed for predicting the strength degradation behavior of materials with either cone cracks or quasi-plastic damage.

From a materials design standpoint, intermediate microstructures may provide the best compromise between opposing requirements of immunity to strength loss from either single-cycle (Fig. 7) or fatigue (Fig. 10) loading and wear resistance. It is clear from the indentation–strength data (Figs. 7, and 10) that full cone cracks can be highly deleterious. On the other hand, excessive quasi-plasticity can also be deleterious, especially under fatigue conditions (Fig. 10), because it

may lead to coalescence of microdamage within the damage zone (Lawn *et al.*, 1998), with consequent material removal (Nagarajan and Jahanmir, 1996). Another manifestation of microcrack coalescence in MGC materials is enhanced machinability (Grossman, 1991).

Finally, it is of interest to examine the results from a clinical standpoint. Fig. 5 indicates values of P_C and P_Y at which the two damage modes first initiate, for a sphere radius of 3.18 mm. [Recall that $r = 3.18$ mm lies within the quoted range 2–4 mm for cuspal radii (Wheeler, 1958).] In Fig. 5, values of P_C for single-cycle loading exceed 600 N, which is well above the level of 200 N often quoted for typical mastication forces (DeLong and Douglas, 1983; Anusavice, 1989; Phillips, 1991; Craig, 1997). However, as seen in the micrographs in Fig. 9, multi-cycle contacts can produce cone cracks at much lower loads, especially in the finer microstructures. Smaller sphere radii can also lower P_C (Lee and Lawn, 1998; Peterson *et al.*, 1998). Once full cone cracks do initiate, strengths are severely degraded, compromising the structure. For quasi-plasticity, the values of P_Y in Fig. 5 actually lie below 200 N over most of the microstructural range. Again, multi-cycle loading can enhance the intensity of quasi-plastic damage, especially in the coarser microstructures. If the damage is sufficiently severe that coalescence occurs, properties can again be severely degraded. Hertzian contact provides a simple route to the simulation of such degradation phenomena, under a variety of potential oral conditions.

ACKNOWLEDGMENTS

The authors thank A. Pajares, H. Cai, A.C. Fischer-Cripps, H.H.K. Xu, S. Jahanmir and J.R. Kelly for fruitful discussions. Participation by S. Wuttiphan was carried out as part of a Ph.D. dissertation, Department of Materials and Nuclear Engineering, University of Maryland, College Park, MD. This work was funded under NIDR Grant PO1 DE10976.

Received September 9, 1997

Address correspondence and reprint request to:

I. M. Peterson

Materials Science & Engineering Laboratory
National Institute of Standards and Technology
Gaithersburg, MD 20899, USA.

Tel.: 301-975-5776;

Fax: 301-975-5012;

E-mail: irene.peterson@nist.gov

REFERENCES

- Anusavice KJ (1989). Criteria for selection of restorative materials: properties vs technique sensitivity. In: *Quality Evaluations of Dental Restorations*. Anusavice KJ, editor. Chicago: Quintessence, pp. 15–56.
- Cai H, Kalceff MAS, Hooks BM, Lawn BR, Chyung K (1994). Cyclic fatigue of a mica-containing glass-ceramic at Hertzian contacts. *J Mater Res* 9:2654–2661.
- Cai H, Stevens Kalceff MA, Lawn BR (1994). Deformation and fracture of mica-containing glass-ceramics in Hertzian contacts. *J Mater Res* 9:762–770.
- Chyung CK, Beall GH, Grossman DG (1972). Microstructures and mechanical properties of mica glass-ceramics. In: *Electron Microscopy and Structure of Materials*. Thomas G, Fulrath RM, Fisher RM, editor. Berkeley, CA: University of California Press, pp. 1167–1194.
- Chyung CK, Beall GH, Grossman DG (1974). Fluorophlogopite mica glass-ceramics. In: *Proceedings of 10th International Glass Congress, No. 14*, Kunugi M, Tashiro M, Saga N, editor. Tokyo, Japan. The Ceramic Society of Japan, Kyoto, pp. 33–40.
- Craig RG (1997). Mechanical properties. In: *Restorative Dental Materials*. Craig RG, editor. St. Louis, MO: Mosby, Chapter 4.
- Davies RM (1949). Determination of static and dynamic yield stresses using a steel ball. *Proc Roy Soc Lond A* 197:416–432.
- DeLong R, Douglas WH (1983). Development of an artificial oral environment for the testing of dental restoratives: bi-axial force and movement control. *J Dent Res* 62:32–36.
- Denry IL, Holloway JA, Gourlaouen V, Johnston WM, Rosenstiel SF (1996). Hertzian indentation response of mica-containing dental glass-ceramics (Abstract # 858). *J Dent Res* 75:125.
- Denry IL, Rosenstiel SF (1995). Hertzian indentation response of Dicor machinable glass-ceramics (Abstract # 976). *J Dent Res* 74:522.
- Fischer-Cripps AC, Lawn BR (1996). Indentation stress-strain curves for "quasi-ductile" ceramics. *Acta Metallurgica et Materiala* 44:519–527.
- Fischer-Cripps AC, Lawn BR (1996). Stress analysis of contact deformation in quasi-plastic ceramics. *J Am Ceram Soc* 79:2609–2618.
- Frank FC, Lawn BR (1967). On the theory of Hertzian fracture. *Proc Roy Soc Lond A* 299:291–306.
- Grossman DG (1991). Structure and physical properties of Dicor/MGC glass-ceramic. In: *Proceedings of the International Symposium on Computer Restorations*, Mörmann WH, editor. Quintessence Publishing Co., Chicago, IL, pp. 103–115.
- Guiberteau F, Pature NP, Cai H, Lawn BR (1993). Indentation fatigue: a simple cyclic Hertzian test for measuring damage accumulation in polycrystalline ceramics. *Philos Mag* A68:1003–1016.
- Guiberteau F, Pature NP, Lawn BR (1994). Effect of grain size on Hertzian contact in alumina. *J Am Ceram Soc* 77:1825–1831.
- Hertz H (1896). Hertz's miscellaneous papers. London, Chs. 5,6.
- Johnson KL (1985). *Contact mechanics*. London: Cambridge University Press.
- Langitan FB, Lawn BR (1969). Hertzian fracture experiments on abraded glass surfaces as definitive evidence for an energy balance explanation of Auerbach's law. *J Appl Phys* 40:4009–4017.
- Lawn BR (1993). *Fracture of brittle solids*. Cambridge: Cambridge University Press, Ch. 9.

- Lawn BR, Lee SK, Peterson IM, Wuttiphan S (1998). A model of strength degradation from Hertzian contact damage in tough ceramics. *J Am Ceram Soc* 81:1509–1520.
- Lawn BR, Marshall DB (1988). Nonlinear stress-strain curves for solids containing closed cracks with friction. *J Mech Phys Solids* 46:85–113.
- Lawn BR, Padture NP, Cai H, Guiberteau F (1994). Making ceramics 'ductile'. *Science* 263:1114–1116.
- Lawn BR, Wiederhorn SM, Roberts DE (1984). Effect of sliding friction forces on the strength of brittle materials. *J Mater Sci* 19:2561–2569.
- Lawn BR, Wilshaw TR (1975). Indentation fracture: principles and applications. *J Mater Sci* 10:1049–1081.
- Lee SK, Lawn BR (1998). Role of microstructure in Hertzian contact damage in silicon nitride: II. strength degradation. *J Am Ceram Soc* 81:997–1003.
- Lee SK, Wuttiphan S, Lawn BR (1997). Role of microstructure in Hertzian contact damage in silicon nitride: I. mechanical characterization. *J Am Ceram Soc* 80:2367–2381.
- Marshall DB, Lawn BR (1980). Flaw characteristics in dynamic fatigue: the influence of residual contact stresses. *J Am Ceram Soc* 63:532–536.
- Mikosza AG, Lawn BR (1971). Section-and-etch study of Hertzian fracture mechanics. *J Appl Phys* 42:5540–5545.
- Mulhearn TO (1959). The deformation of metals by Vickers-type pyramidal indenters. *J Mech Phys Solids* 7:85–96.
- Nagarajan VS, Jahanmir S (1996). Relationship between microstructure and wear of mica-containing glass-ceramics. *Wear* 200:176–185.
- Padture NP, Lawn BR (1994). Toughness properties of a silicon carbide with an in-situ-induced heterogeneous grain structure. *J Am Ceram Soc* 77:2518–2522.
- Peterson IM, Pajares A, Lawn BR, Thompson VP, Rekow ED (1998). Mechanical Characterization of Dental Ceramics Using Hertzian Contacts. *J Dent Res* 77:589–602.
- Phillips R (1991). Skinner's science of dental materials. Philadelphia, PA: W.B. Saunders.
- Roesler FC (1956). Brittle fractures near equilibrium. *Proc Phys Soc Lond* B69:981–992.
- Tabor D (1951). Hardness of metals. Oxford: Clarendon.
- Wheeler RC (1958). A textbook of dental anatomy and physiology. Philadelphia, PA: W.B. Saunders, pp. 354–358.
- Wilshaw TR (1971). The Hertzian fracture test. *J Phys D: Appl Phys* 4:1567–1581.
- Xu HHK, Smith DT, Jahanmir S (1996). Influence of microstructure on indentation and machining of dental glass-ceramics. *J Mater Res* 11:2325–2337.